INTERNATIONAL JOURNAL FOR NUMERICAL METHODS IN FLUIDS
Int. J. Numer. Meth. Fluids 2005; **47**:491–516
Published online 14 December 2004 in Wiley InterScience (www.interscience.wiley.com). DOI: 10.1002/fld.827

Numerical simulations of transonic aerodynamic flows based on a hierarchical formulation

Mohamed Hafez*,† and Essam Wahba

University of California, Davis CA 95646, U.S.A.

SUMMARY

In this paper, steady two-dimensional potential flows over airfoils are calculated with and without entropy and vorticity corrections, due to the presence of shock waves and/or laminar boundary layers. The results are in agreement with the corresponding solutions of Euler and Navier–Stokes equations. The present approach is briefly described and some extensions are discussed. Copyright © 2004 John Wiley & Sons, Ltd.

KEY WORDS: viscous and inviscid transonic flows; Helmholtz decomposition

1. INTRODUCTION

The breakthrough of Murman and Cole in 1971 opened the door for a flood of papers on transonic flow simulations. Small disturbance equation was used as a model featuring the necessary non-linearity and the mixed type nature of transonic flows with shocks. Later, Murman introduced a conservative scheme to capture correctly embedded and bow shocks. Moreover, Engquist and Osher constructed a scheme satisfying a generalized entropy condition on the discrete level. Extensions to the solution of the full potential equation followed by Jameson and others for two and three-dimensional flows. For a comprehensive review of these developments see References [1, 2]. The type dependent discretization schemes and relaxation procedures introduced for the solution of the potential equation had some advantages in terms of accuracy and efficiency compared to the solution of Euler equations at that time, where the unsteady hyperbolic equations with artificial viscosity terms added everywhere in the field, were solved explicitly to reach a steady state solution. During the eighties there were intensive efforts to improve the solution procedures of Euler equations, as a prerequisite to the solution of Navier–Stokes equations for the high Reynolds number flows. Implicit schemes introduced by Beam and Warming, MacCormack and Lerat improved the efficiency of calculations. Local time stepping, residual smoothing and multigrid as well as preconditioning techniques

*Correspondence to: M. Hafez, University of California, Davis CA 95646, U.S.A.
†E-mail: mhafez@ucdavis.edu

Received 28 January 2004
Revised 16 July 2004

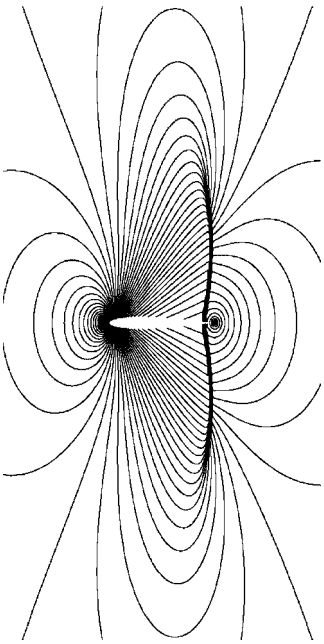

Figure 1. C_p contours (potential flow, $M_\infty = 0.86$, $\alpha = 0^\circ$).

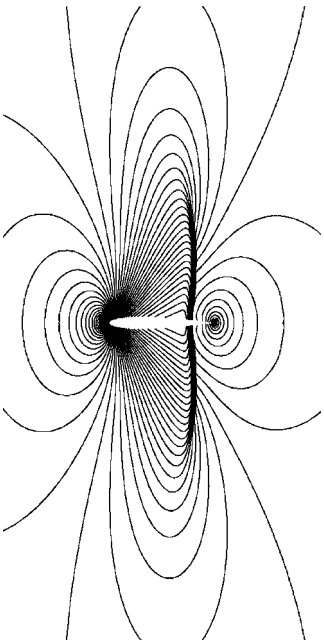

Figure 2. C_p contours (rotational flow, $M_\infty = 0.86$, $\alpha = 0^\circ$).

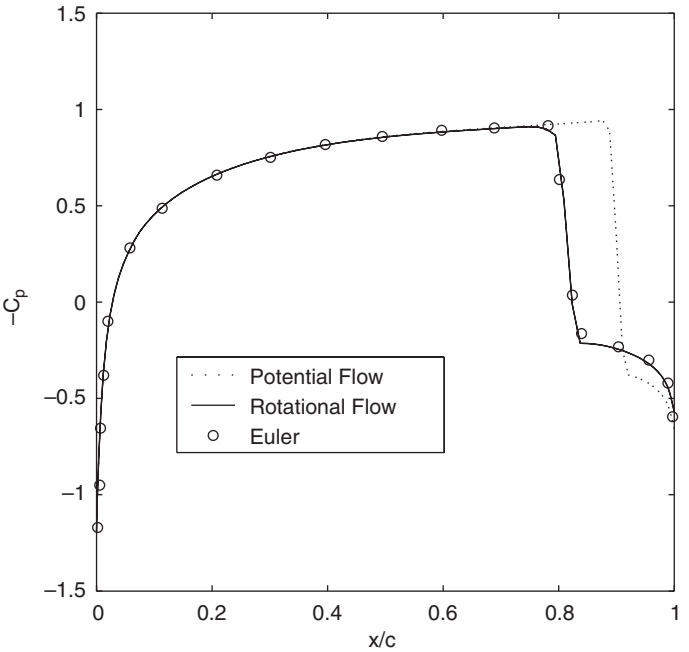

Figure 3. C_p on the surface ($M_\infty = 0.86$, $\alpha = 0^\circ$) (Euler results from Reference [9]).

and GMRES are used for convergence acceleration. Fourth order dissipation was introduced early by Kreiss for the solution of hyperbolic equations with smooth solutions. Blending second and fourth order dissipation terms of a finite volume formulation was introduced by MacCormack and used also by Jameson, Turkel and Schmit with methods of lines based on a multistage Runge–Kutta time integration method. The use of limiters and TVD schemes enhanced the calculations further. On the other hand, Godunov type schemes based on the exact and approximate solutions of the exact and approximate Riemann problems were developed by van Leer, Roe and Osher. Later, high resolution schemes and essentially non-oscillatory schemes were introduced by Harten and others. For more details see [1]. The recent multidimensional upwinding and fluctuations splitting schemes are also promising [3]. Both block structured and unstructured grids were used in flow simulations based on Euler equations over complex geometries. Recently, finite elements methods become competitive to finite volumes, see for example Morgan *et al.* [4]. The first transonic flow simulation over a complete airplane was accomplished by Glowinski *et al.* based on a control theory formulation of potential flow. For more details see References [5, 6]. Most of the Euler schemes discussed here, have been used for the solution of Navier–Stokes equations, starting with Lax–Wandroff schemes, MacCormack explicit and implicit schemes including the bidiagonal scheme, the line relaxation and the recent symmetric schemes, Jameson's method of lines with scalar and matrix dissipation and Beam and Warming ADI scheme, Lerat implicit schemes, as well as, upwind schemes, in particular Roe flux difference splitting for the discretization of the convection terms. Similarly, finite elements have been used for the simulation of high Reynolds number viscous flows with structured grids in the boundary layers and the wakes and unstructured grids

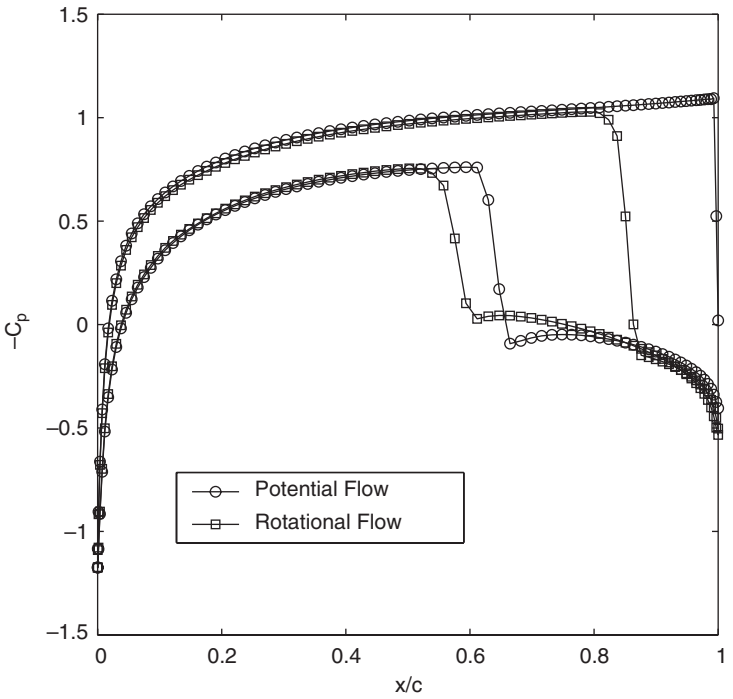

Figure 4. C_p on the surface ($M_\infty = 0.85,\ \alpha = 1^\circ$).

in the inviscid flow regions. Potential, Euler and Navier–Stokes codes have been successfully used in industry. Nevertheless, there is still a need for more developments as described by a recent paper by Johnson *et al.* [7]. In the present paper, we will present numerical results for 2-D transonic flows over airfoils based on a hierarchical approach using a potential formulation with corrections due to entropy and vorticity generated by curved shocks and/or viscous layers. The motivation behind the present approach is to exploit the fact that entropy and vorticity are confined to relatively small domains for most external aerodynamic flows, even at off design conditions. The base calculations are produced using a potential solver based on flux upwinding [8]. The modifications to account for entropy and vorticity variations are introduced to satisfy the momentum equations. In the following, the details of the formulation for inviscid and viscous flows are derived and the numerical methods are described followed by a discussion of the results.

2. A HIERARCHICAL FORMULATION FOR INVISCID ADIABATIC FLOWS

Ignoring viscous effects and heat transfer, Navier–Stokes equations reduce to Euler equations representing conservation of mass, momentum and energy. For steady two dimensional flows,

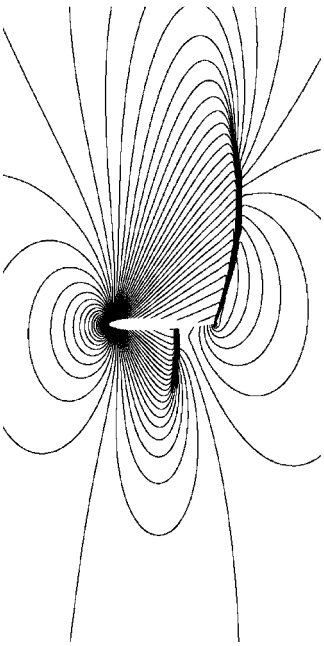

Figure 5. C_p contours (potential flow, $M_\infty = 0.85$, $\alpha = 1^\circ$).

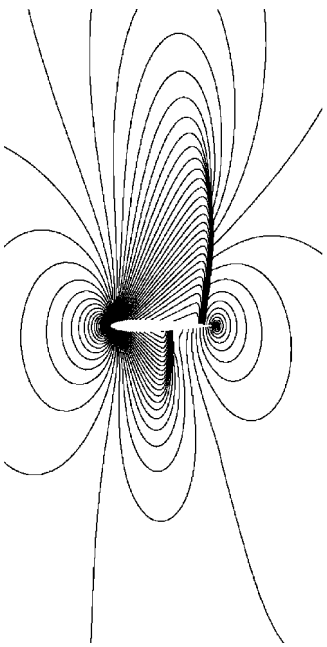

Figure 6. C_p contours (rotational flow, $M_\infty = 0.85$, $\alpha = 1^\circ$).

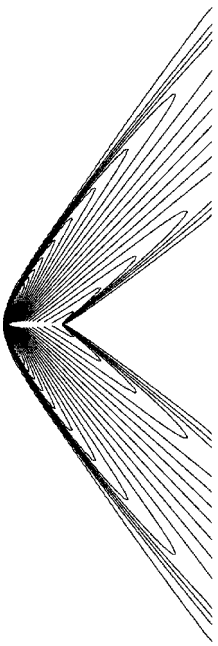

Figure 7. C_p contours (potential flow, $M_\infty = 1.4$, $\alpha = 0^\circ$).

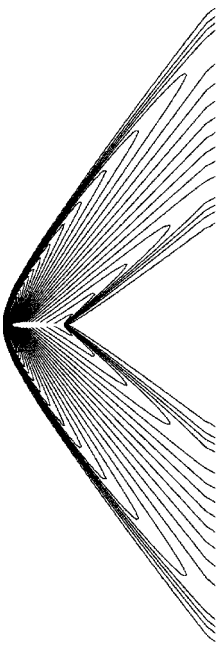

Figure 8. C_p contours (rotational flow, $M_\infty = 1.4$, $\alpha = 0^\circ$).

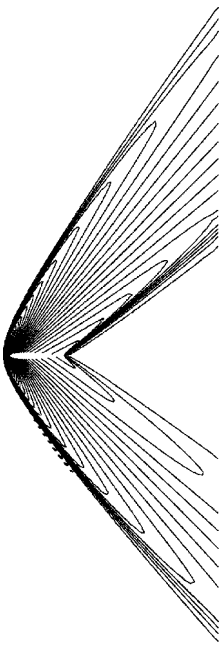

Figure 9. C_p contours (potential flow, $M_\infty = 1.4,\ \alpha = 4^\circ$).

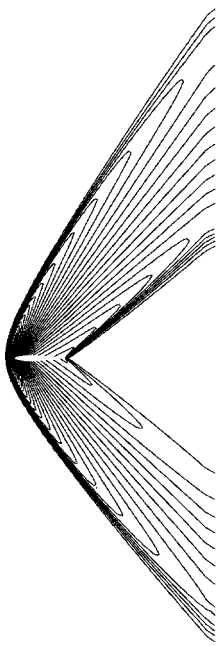

Figure 10. C_p contours (rotational flow, $M_\infty = 1.4,\ \alpha = 4^\circ$).

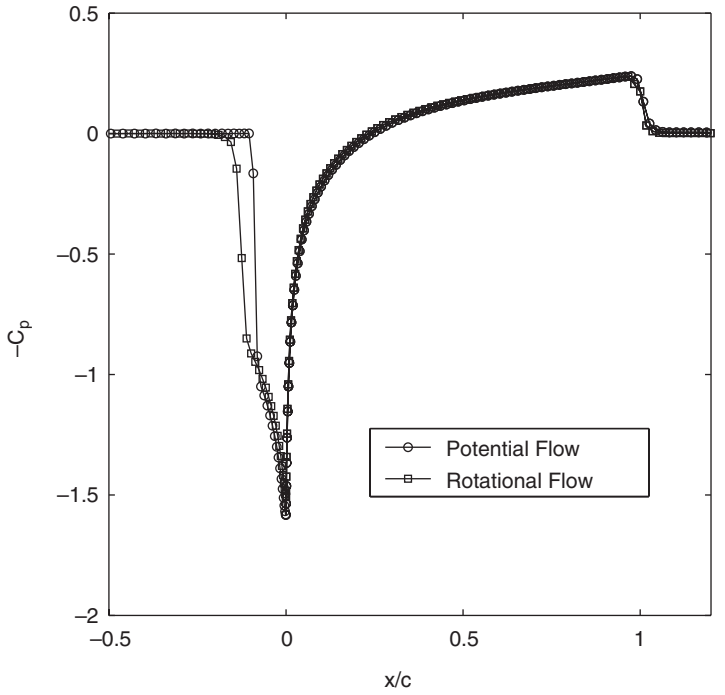

Figure 11. C_p on the surface ($M_\infty = 1.4$, $\alpha = 0^\circ$).

the governing equations for a perfect gas, in standard notations, are given by

$$\nabla \cdot \rho \boldsymbol{q} = 0 \tag{1}$$

$$\nabla \cdot \rho \boldsymbol{q}\boldsymbol{q} = -\nabla P \tag{2}$$

$$\nabla \cdot \rho \boldsymbol{q} H = 0 \tag{3}$$

where H is the total enthalpy

$$H = \frac{\gamma}{\gamma - 1}\frac{p}{\rho} + \frac{1}{2}q^2 \tag{4}$$

For uniform upstream conditions and excluding closed streamlines, Equation (3) implies that H is uniformly constant everywhere in the field. For the case of variable upstream conditions, for example gust, H remains constant along a streamline, but it varies from one streamline to another. For smooth flows, the momentum equations can be rewritten in the Lamb form:

$$\boldsymbol{\omega} \times \boldsymbol{q} = T\nabla S - \nabla H \tag{5}$$

Equation (5) implies that, the entropy, S, is constant along a streamline ($\psi = constant$). However, S jumps across shocks. Equation (5) implies also that the vorticity is related to the gradient of entropy and total enthalpy normal to the streamline direction. For two-dimensional

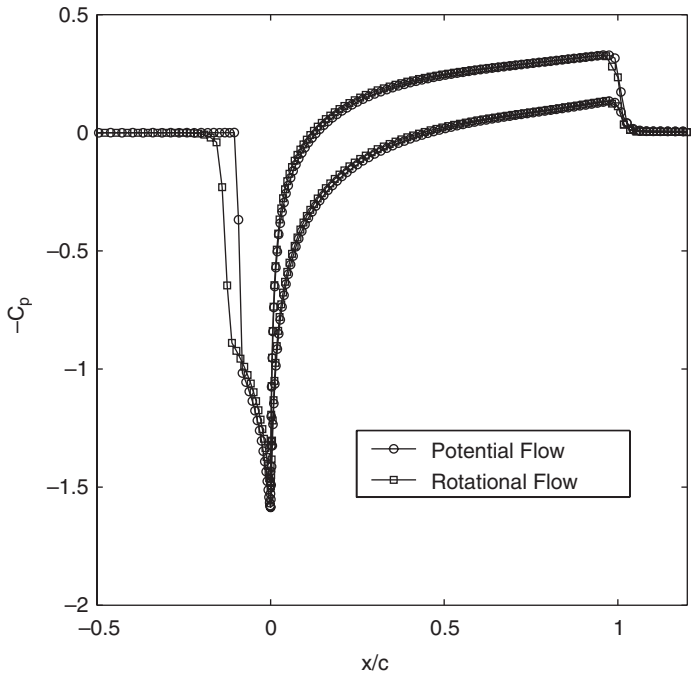

Figure 12. C_p on the surface ($M_\infty = 1.4$, $\alpha = 4^\circ$).

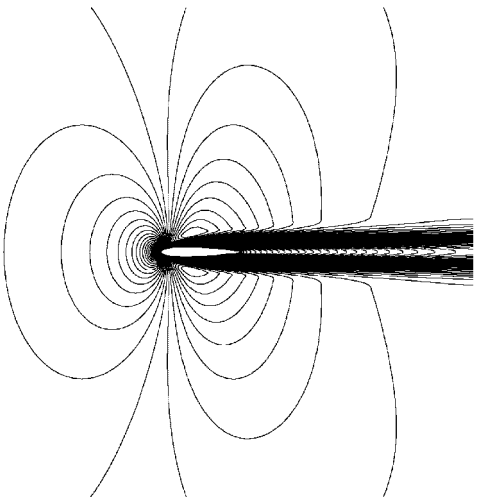

Figure 13. Mach contours ($M_\infty = 0.8$, $Re = 500$, $\alpha = 0^\circ$).

flows equation (5) reduces to

$$\omega = P\,\frac{\partial S/R}{\partial \psi} - \rho\,\frac{\partial H}{\partial \psi} \tag{6}$$

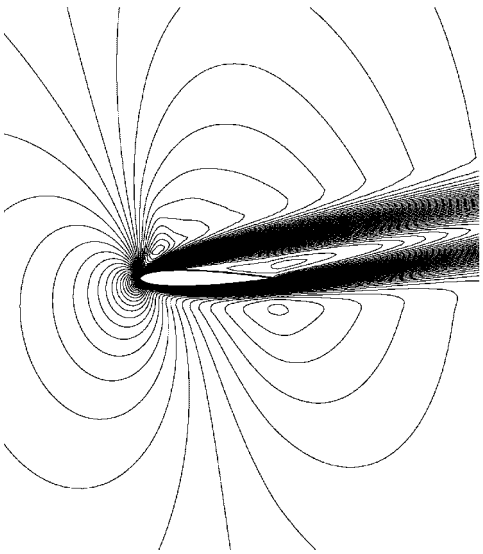

Figure 14. Mach contours ($M_\infty = 0.8$, $Re = 500$, $\alpha = 10^\circ$).

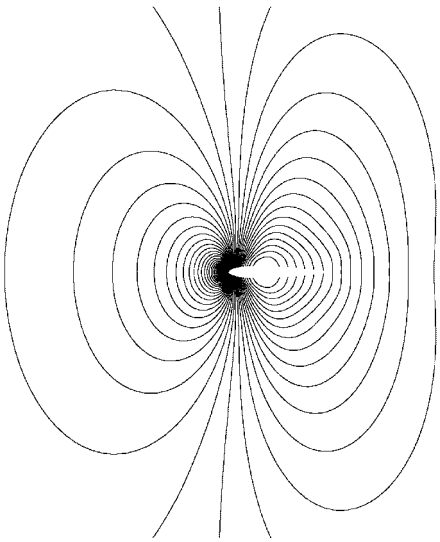

Figure 15. C_p contours ($M_\infty = 0.8$, $Re = 500$, $\alpha = 0^\circ$).

Hence, for constant total enthalpy, ω/P is constant along a streamline, while ω/ρ is constant along a streamline for constant entropy, i.e. isentropic flow. For regions where both H and S are constant the vorticity vanishes, i.e. the flow is irrotational. This is the case in the far field, excluding the wake, of most external aerodynamics flows. To take advantage of this

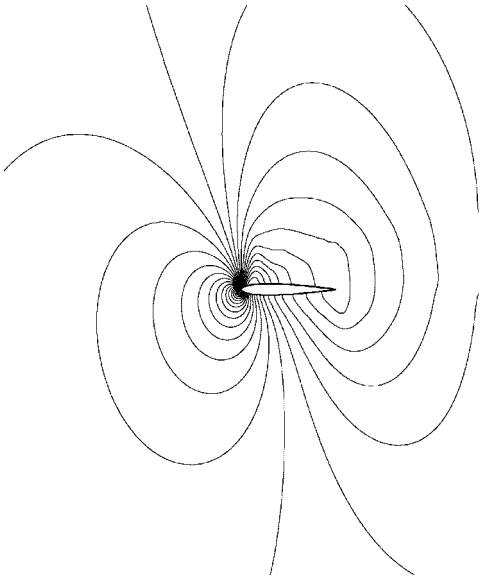

Figure 16. C_p contours ($M_\infty = 0.8$, $Re = 500$, $\alpha = 10^\circ$).

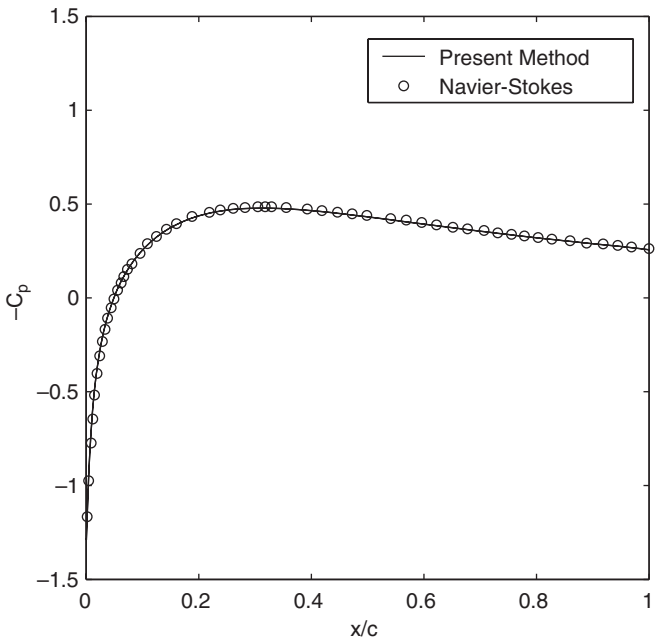

Figure 17. C_p on the surface ($M_\infty = 0.8$, $Re = 500$, $\alpha = 0^\circ$) (Navier–Stokes results from Reference [10]).

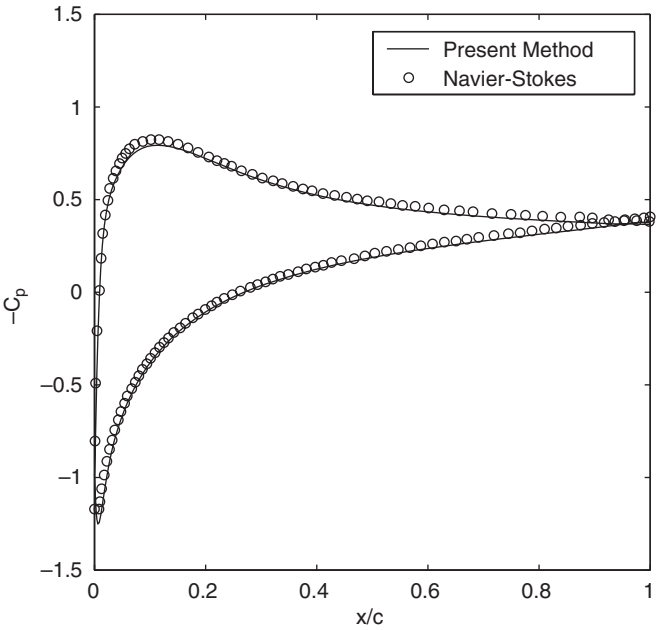

Figure 18. C_p on the surface ($M_\infty = 0.8$, $Re = 500$, $\alpha = 10^\circ$) (Navier–Stokes results from Reference [10]).

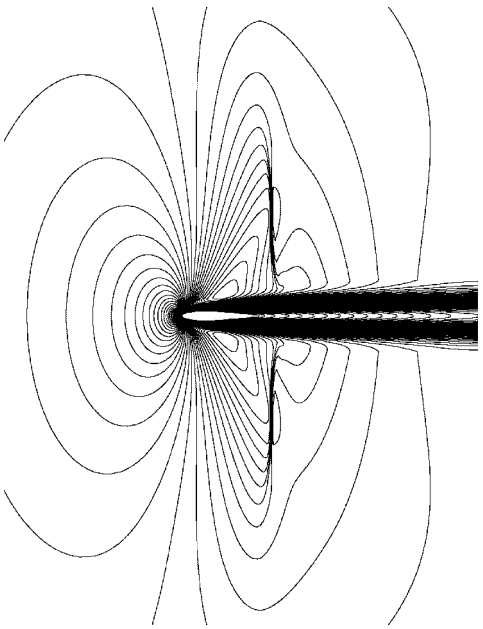

Figure 19. Mach contours ($M_\infty = 0.9$, $Re = 500$, $\alpha = 0^\circ$).

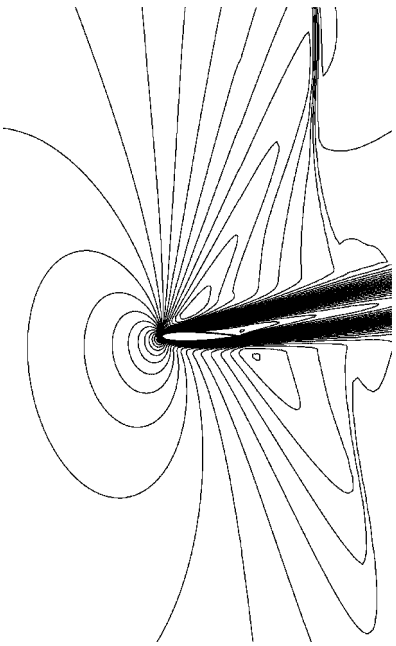

Figure 20. Mach contours ($M_\infty = 0.9$, $Re = 500$, $\alpha = 10^\circ$).

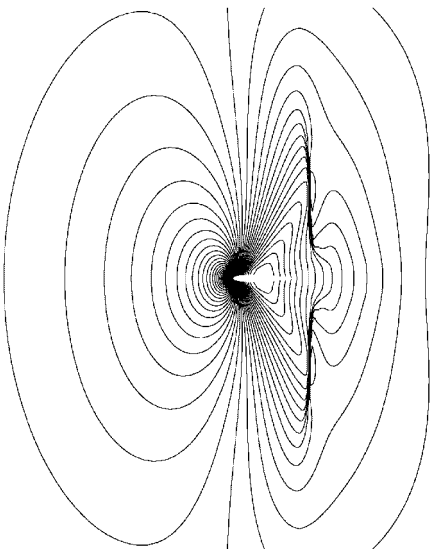

Figure 21. C_p contours ($M_\infty = 0.9$, $Re = 500$, $\alpha = 0^\circ$).

fact, several formulations, in terms of vorticity, have been proposed in the past. In References [9–12] generalized Cauchy/Riemann equations were solved assuming entropy and vorticity are known. The latter are updated to satisfy the tangential and normal momentum equations. See

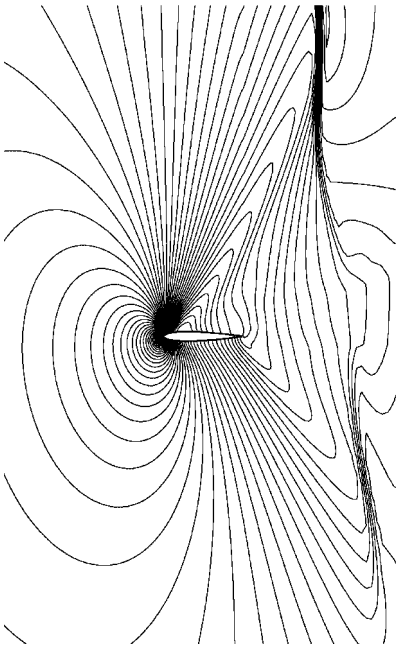

Figure 22. C_p contours ($M_\infty = 0.9$, $Re = 500$, $\alpha = 10^\circ$).

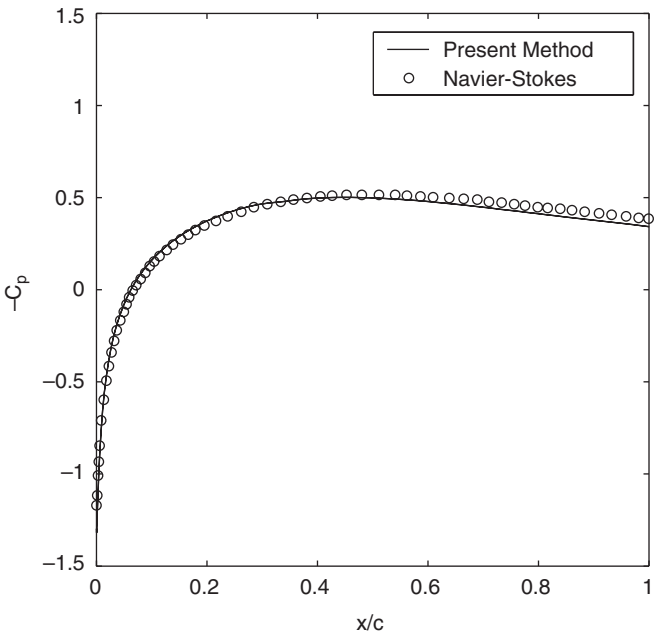

Figure 23. C_p on the surface ($M_\infty = 0.9$, $Re = 500$, $\alpha = 0^\circ$) (Navier–Stokes results from Reference [10]).

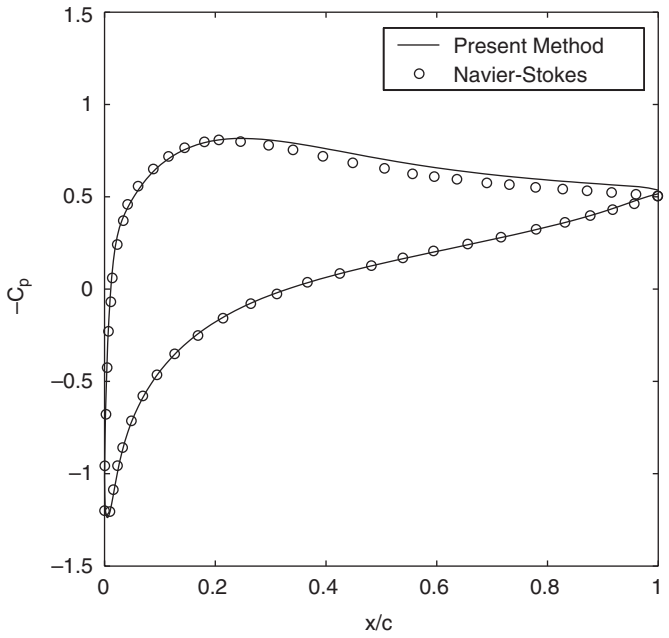

Figure 24. C_p on the surface ($M_\infty = 0.9$, $Re = 500$, $\alpha = 10^\circ$) (Navier–Stokes results from Reference [10]).

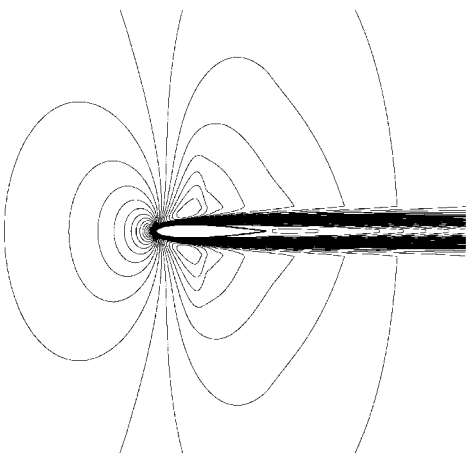

Figure 25. Mach contours ($M_\infty = 0.85$, $Re = 2000$, $\alpha = 0^\circ$).

also the work of Johnson *et al.* [13]. The present work depends on a velocity decomposition similar to that introduced by Helmholtz. Other options are also possible. For example, in Reference [14] a multiplicative correction to the gradient of the potential is used instead. Here the velocity vector is split into a gradient of a potential plus a rotational component,

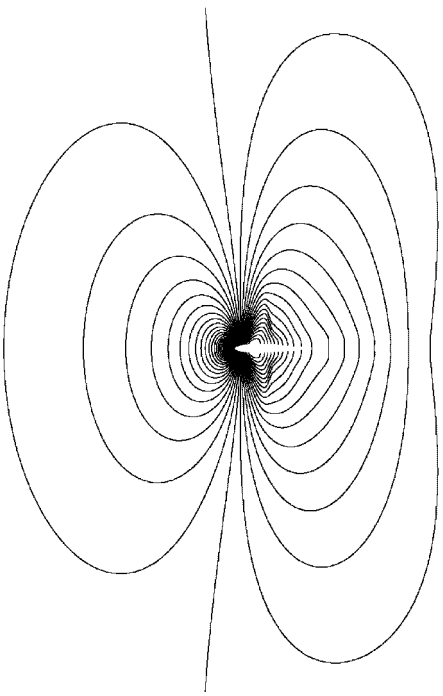

Figure 26. C_p contours ($M_\infty = 0.85$, $Re = 2000$, $\alpha = 0^\circ$).

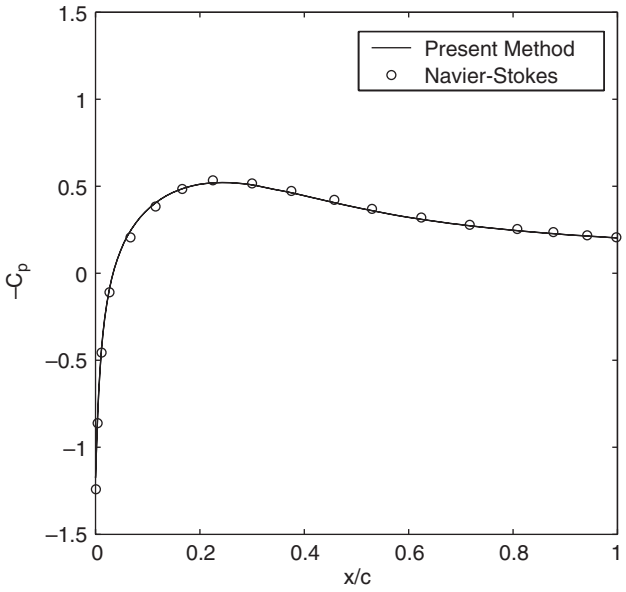

Figure 27. C_p on the surface ($M_\infty = 0.85$, $Re = 2000$, $\alpha = 0^\circ$) (Navier–Stokes results from Reference [30]).

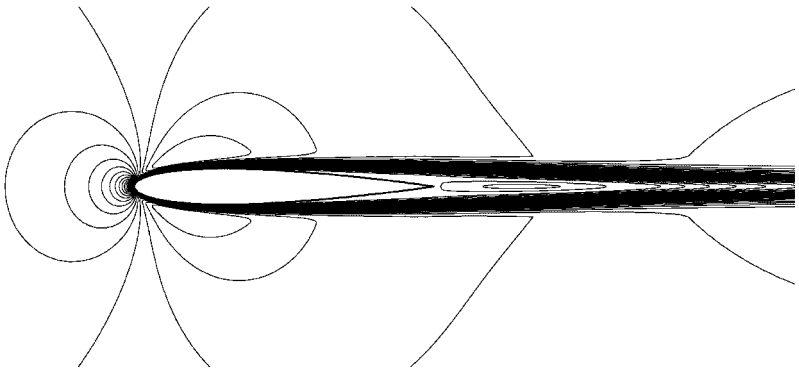

Figure 28. Mach contours ($M_\infty = 0.5$, $Re = 10\,000$, $\alpha = 0^\circ$).

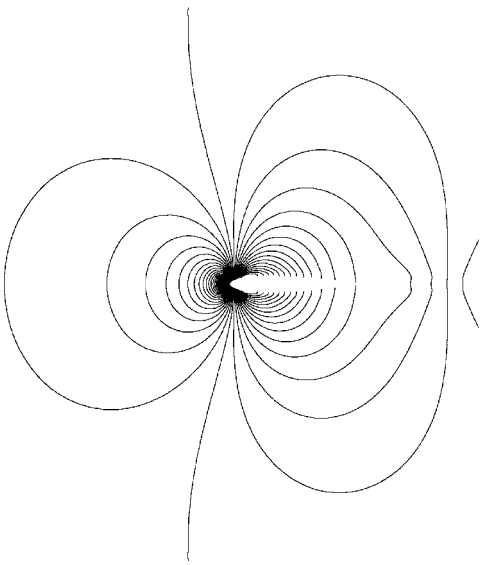

Figure 29. C_p contours ($M_\infty = 0.5$, $Re = 10\,000$, $\alpha = 0^\circ$).

namely

$$\boldsymbol{q} = \nabla\phi + \boldsymbol{q}^* \tag{7}$$

Hence,

$$\boldsymbol{\omega} = \nabla \times \boldsymbol{q} = \nabla \times \boldsymbol{q}^* \tag{8}$$

The continuity equation becomes

$$\nabla \cdot \rho\nabla\phi = -\nabla \cdot \rho\boldsymbol{q}^* \tag{9}$$

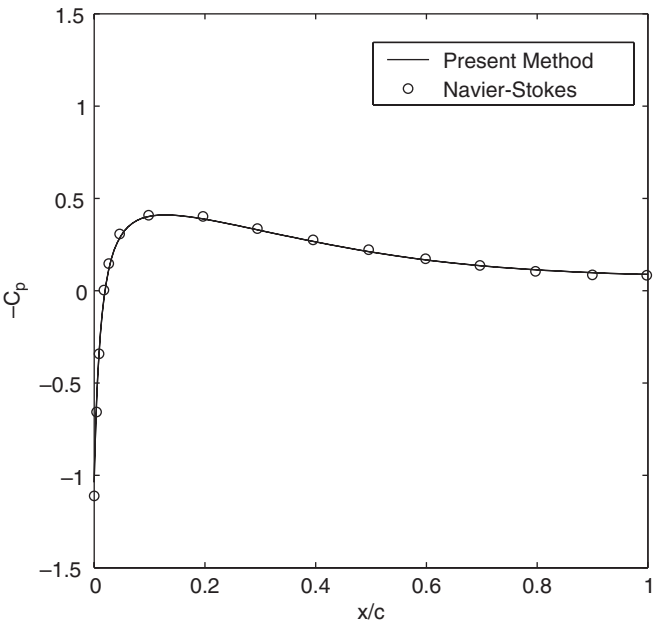

Figure 30. C_p on the surface ($M_\infty = 0.5$, $Re = 10\,000$, $\alpha = 0^\circ$) (Navier–Stokes results from Reference [31]).

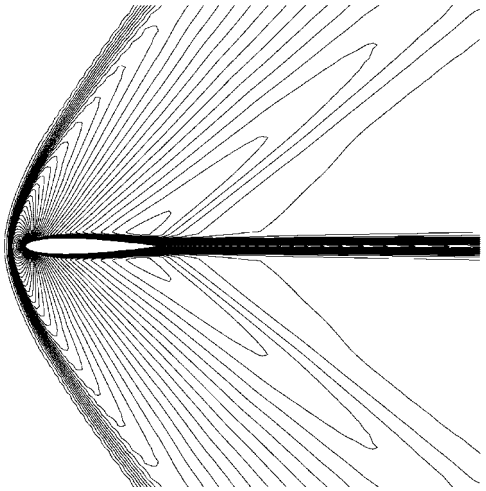

Figure 31. Mach contours ($M_\infty = 1.5$, $Re = 1 \times 10^4$, $\alpha = 0^\circ$).

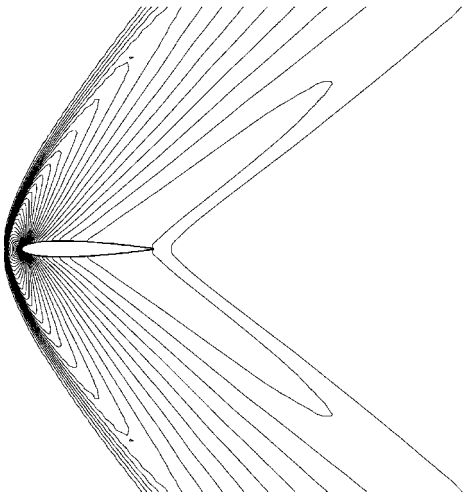

Figure 32. C_p contours ($M_\infty = 1.5$, $Re = 1 \times 10^4$, $\alpha = 0^\circ$).

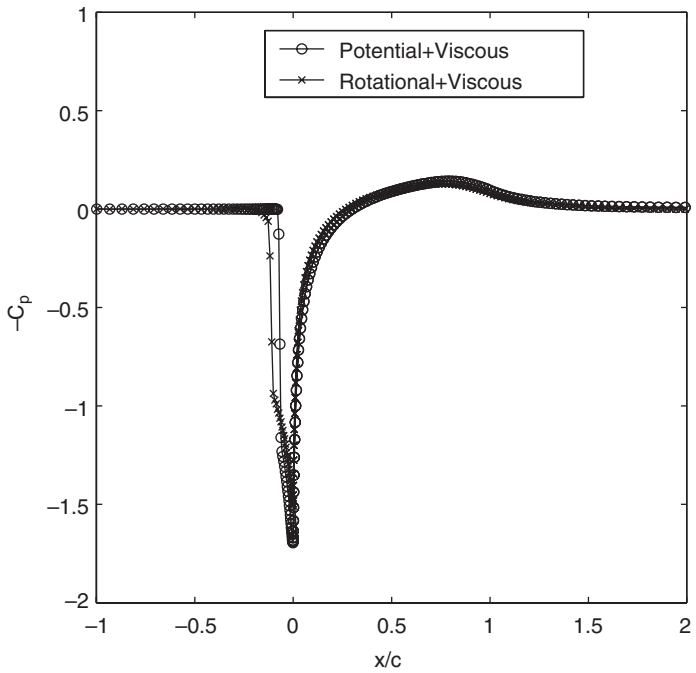

Figure 33. C_p at the axis ($M_\infty = 1.5$, $Re = 1 \times 10^4$, $\alpha = 0^\circ$).

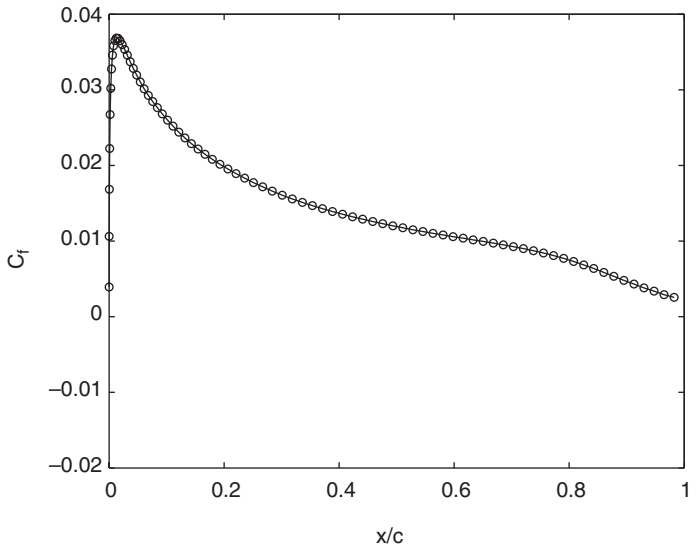

Figure 34. C_f on the body ($M_\infty = 1.5$, $Re = 1 \times 10^4$, $\alpha = 0^\circ$).

The right hand side of Equation (9) is a source term to account for the contribution of the rotational velocity component to the conservation of mass. The energy equation is represented by the statement

$$H = H_\infty = \frac{1}{\gamma - 1}\frac{1}{M_\infty^2} + \frac{1}{2} \tag{10}$$

where the velocity has been made dimensionless based on q_∞ and the total enthalpy based on q_∞^2. The pressure and the density of non-isentropic flows can be represented by

$$P = P_i e^{-\Delta S/R}, \quad \rho = \rho_i e^{-\Delta S/R}, \quad P_i = \frac{\rho_i^\gamma}{\gamma M_\infty^2} \tag{11}$$

Hence,

$$\frac{\gamma}{\gamma - 1}\frac{P_i}{\rho_i} + \frac{1}{2}q^2 = H_\infty \tag{12}$$

Equation (12) provides ρ_i and P_i in terms of q^2. To complete the formulation, we need the entropy S and the rotational component of the velocity $\boldsymbol{q}^*$. For two-dimensional flows, the vorticity vector is normal to the plane, hence only its magnitude is unknown. Therefore, the magnitude of $\boldsymbol{q}^*$, or one of its components, can be obtained by integrating the vorticity definition given by Equation (8). The vorticity and the entropy can be obtained from the momentum equations. Specifically, a combination of the x- and y-momentum equations in either the flow direction or in a direction tangent to grid lines (if the grid is almost aligned with the flow) is used to calculate the entropy correction, while the correction to the magnitude of $\boldsymbol{q}^*$, or its components is calculated to enforce another combination of the momentum equations in a direction normal to the flow direction. For unstructured grids, one can use the direction of

the pseudo potential flow and its normal, to calculate the above-mentioned corrections. The present formulation is completely equivalent to Euler equations. It includes potential flow as a special case, if entropy terms and the rotational component of the velocity are dropped. We can also include only the entropy corrections and ignore the vorticity, if the shock curvature is negligible [15, 16]. The isentropic Euler equations can be also obtained if the pressure is calculated from the normal momentum equations and the rotational component of the velocity from the tangential momentum equation while the energy equation is replaced by the isentropic relation, which in turn, provides the density. All these levels of approximations are subsets or special cases, which can be valid locally in some regions of the flow field. The main point here is the use of the potential flow as a base for the calculations with local corrections, not necessarily small in magnitude, but limited to relatively small domains. Exact integration of the momentum and energy equations avoids generation of artificial entropy and vorticity from truncation errors particularly on coarse meshes, unless special schemes are developed to preserve these quantities. Even then, one must detect where to apply such schemes, since entropy should be generated from shock waves and a scheme which preserves entropy everywhere is good only for flows without shocks. Schemes which conserve automatically potential flows are developed in Reference [17].

3. A HIERARCHICAL FORMULATION FOR VISCOUS FLOW WITH HEAT CONDUCTION

There have been many attempts to simulate viscous flows at high Reynolds numbers based on viscous/inviscid interaction procedures. The first was proposed by Prandtl, coupling potential flows with boundary layers using the concept of displacement thickness, such that at each station on the airfoil the inviscid mass flow rate over the displaced body is equal to the viscous mass flow rate over the original body. The inviscid flow calculation, in turn, over the augmented body provides the surface pressure gradient in the streamwise direction, which is imposed as a forcing function in the tangential momentum equation of the boundary layer calculations. The coupling between the potential flows and boundary layers is crucial for the overall convergence of any iterative procedure to solve the combined problem. It is difficult, however, to construct a robust procedure for attached and separated flows in both sub and supersonic regions [18–23]. Other difficulties exist with boundary layer approximations, at least from theoretical point of view, at the leading and trailing edges and at separation and attachment points. Moreover, extensions to three-dimensional flows over wings are not straightforward, in particular at the tips and wing-body junctions. Because of all these issues, zonal methods were introduced where Navier–Stokes equations are solved in the neighbourhood of the body and in the wake and Euler or potential equations are solved outside the viscous layers, as in heterogeneous domain decomposition methods [24–26]. Again, convergence difficulties are usually encountered due to the reflection of the error from the artificial interface between the two regions where different equations are solved [27, 28]. Some of these problems are avoided in our hierarchical formulation, which is equivalent to Navier–Stokes equations. The Navier–Stokes equations, for steady laminar flows of a perfect gas, are:

$$\nabla \cdot \rho \boldsymbol{q} = 0 \tag{13}$$

$$\nabla \cdot \rho \boldsymbol{q}\boldsymbol{q} = -\nabla P + \frac{1}{Re} \nabla \cdot \tau \tag{14}$$

$$\nabla \cdot \rho \boldsymbol{q} H = \frac{1}{Re\, Pr} \nabla \cdot k \nabla T + \frac{1}{Re} \nabla \cdot \boldsymbol{q} \cdot \tau \tag{15}$$

where τ is the viscous stress tensor and k is the non-dimensional heat conductivity of the fluid. The two parameters in the energy equations are the Reynolds (Re) and Prandtl (Pr) numbers. For high Reynolds number flows, the viscous stresses and the heat transfer are confined to the boundary layers and wakes. Outside these regions, Euler equations are valid, where the total enthalpy is constant with uniform upstream conditions. On the other hand, inside the boundary layers and the wake, the total enthalpy can be considered constant if $Pr = 1$ [10]. Hence, one can use constant total enthalpy for high Reynolds number flows everywhere, even inside the viscous layers. For convenience, we will replace Equation (15) by Equation (10).

$$H = C_p T + \frac{1}{2} q^2 = H_\infty = \frac{1}{\gamma - 1} \frac{1}{M_\infty^2} + \frac{1}{2} \tag{16}$$

Such an approximation implies that the body surface temperature is constant and there is no heat transfer through the body surface (i.e. $\partial T/\partial n = 0$). In general, Equation (15) must be solved for H. As in inviscid flows, the same decomposition of the velocity into a gradient of a potential plus a rotational component, Equation (7), is adopted. The conservation of mass is still given by Equation (9). The right hand side represents distributed sources to account for the displacement effects of the boundary layer on the outer inviscid flow field. The representations of the pressure and density given in Equations (11) and (12) are still valid. Hence, the only difference between the viscous and the inviscid flow calculations are in the momentum equations, which contain now viscous stresses. The latter increase the order of the equation and require the enforcement of the no slip boundary condition in addition to the no penetration condition. In general, conserving the two components of the momentum provides two coupled equations for the two remaining unknowns, the entropy and the rotational velocity component. The strategy for obtaining the corrections to the potential field due to entropy and vorticity inside the viscous layer differs, however, from that used in the inviscid flow region. The normal momentum equation is integrated to obtain the pressure marching from the inviscid flow inward to the surface. The tangential momentum equation is used to update the rotational component. For separated flows, the momentum equations, tangential and normal to the body, are used instead. A unified strategy for both inviscid and viscous flows is possible if the two momentum equations are solved simultaneously in a coupled manner. At any rate, the formulation is equivalent to Navier–Stokes equations for both attached and separated flows.

4. NUMERICAL METHODS AND NUMERICAL RESULTS

Standard numerical methods are used to test the present formulation. First, a fine grid is generated around NACA0012 airfoil based on simple algebraic methods (The results for inviscid flows over a cylinder are reported in Reference [29].) A cell vertex, finite volume scheme is adopted for discretization. Artificial viscosity is added explicitly for numerical stability. Artificial time dependent terms and successive line relaxation procedures are parts of the iterative

solution algorithm. The segregated treatment of the potential equation and the convection diffusion equations for entropy and the rotational velocity component is chosen for simplicity. All the results reported here reached a maximum residual of at least 10^{-8}. Obviously, more powerful techniques are applicable and such a study will be the subject of a separate paper. Numerical results of some benchmark problems are reported for both inviscid and viscous transonic aerodynamic flows. Four cases are presented for NACA0012 airfoil at $M_\infty = 0.85$ and $\alpha = 1°$, $M_\infty = 0.86$ and $\alpha = 0°$, and $M_\infty = 1.4$ for $\alpha = 0$ and $4°$. All these cases have curved shocks generating entropy and vorticity in limited domains. The pressure contours are plotted in Figures 1–12. The surface pressure distributions of isentropic irrotational and non-isentropic rotational flows are compared in Figures 3, 4 and 11, 12. All these solutions are in good agreement with published results available in literature [3].

For viscous flows, several cases are considered. Laminar flows of $Re = 500$ over NACA0012 airfoil at $\alpha = 0, 10°$ and $M_\infty = 0.8, 0.9$ are simulated with the present formulation and the results are plotted in Figures 13–24. Higher Reynolds number cases are presented in Figures 25–30 for $M_\infty = 0.85$, $\alpha = 0°$ and $Re = 2000$ and for $M_\infty = 0.5$, $\alpha = 0°$ and $Re = 10\,000$. A supersonic case is also simulated for $M_\infty = 1.5$, $\alpha = 0°$ and $Re = 10\,000$ and the results are shown in Figures 31–34. Two pressure distributions at the axis are plotted in Figure 33 for coupling potential and rotational flows with the viscous layer. The skin friction for the latter is plotted in Figure 34. The same cases are calculated using standard formulations of Navier–Stokes equations (see References [10, 30–32]). Again, our solutions are in good agreement with the published results.

5. CONCLUDING REMARKS

Alternative formulations to the standard Euler and Navier–Stokes equations can be based on generalized Cauchy/Riemann equations [9–12], stream functions [33, 34], or potential functions with corrections to account for rotational flow fields. In this paper, numerical results are presented based on a hierarchical approach, with the potential flow solver as a base for both inviscid and viscous flows. Test cases with subsonic, transonic and supersonic free streams are considered. The solutions are in good agreement with the results available in literature. Extensions to turbulent flows and massive separation cases will depend on transition and turbulence modelling. The latter is an independent ingredient, necessary for any formulation. Standard numerical techniques have been used in the present study, which are amenable for parallel computations. More powerful procedures are, however, applicable to both the base potential flow solver, and the entropy and vorticity corrections. The extension to three-dimensional flows over wings is currently under development.

APPENDIX A: KUTTA–JOUKOWSKI CONDITION FOR THE SOLUTION OF THE POTENTIAL EQUATION

For potential flow calculations, Kutta–Joukowski condition is imposed to prevent the flow from going around the trailing edge. To guarantee that the pressure is continuous, ϕ_s (upwinded) is enforced to be equal at both sides of the trailing edge. The jump of the potential at the trailing edge is also enforced along the cut all the way to the outer boundary. Moreover, since

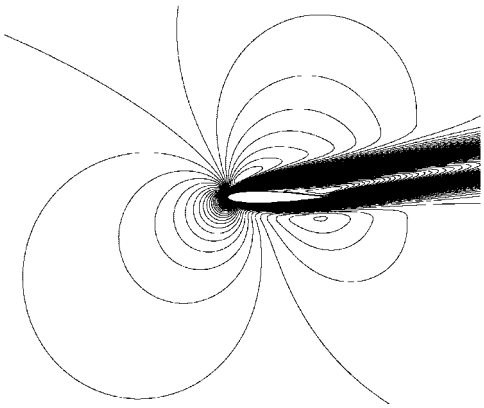

Figure A1. U contours $Re = 500,\ \alpha = 10^\circ$).

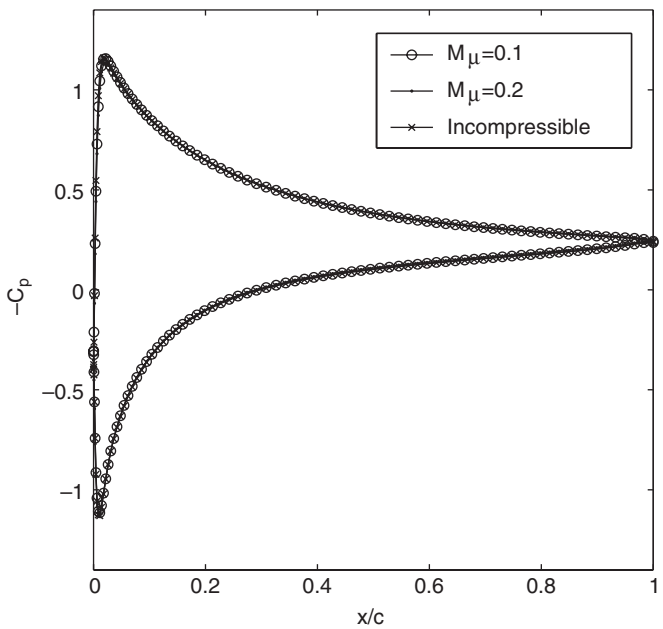

Figure A2. C_p on the body ($M_\infty = 0.0, 0.1, 0.2,\ Re = 500,\ \alpha = 10^\circ$).

the jump of the potential is equal to the circulation in this case, it is used to calculate the far-field boundary condition. The same strategy is used for the calculations of the potential equation with the vorticity correction for both inviscid and viscous flows. Unlike potential flows, inviscid rotational flows leave the airfoil surface tangent to the side of lower entropy because of the vorticity correction. At any rate, the circulation in the far-field is related to the total lift according to Joukowski theorem, even for massively separated flows, provided that the contour used for the evaluation of the circulation is chosen to be perpendicular to the vortical wake.

APPENDIX B: THE INCOMPRESSIBLE FLOW LIMIT

The present formulation has already a built-in preconditioning for the simulation of low Mach number flows. For the case with no heat transfer, the density remains constant as $M_\infty \to 0$. The energy equation decouples and the vorticity component of the velocity is obtained, as before, from the tangential momentum equation. The pressure is calculated from the normal momentum equation and the entropy is not needed in such a procedure. Numerical results are obtained for NACA0012 airfoil at $M_\infty = 0.0, 0.1, 0.2$ with $\alpha = 10^\circ$ and $Re = 500$. In Figures A1 and A2, the u-velocity contours and the surface pressure distributions are plotted for the three cases. The same rate of convergence was observed for incompressible and compressible flows. Moreover, no degeneration of accuracy is noticed for the incompressible flow case.

REFERENCES

1. Hirsch C. *Numerical Computation of Internal and External Flows* 1990; **1,2**.
2. Holst T. Transonic flow computations using nonlinear potential methods. *Progress in Aerospace Sciences* 2000; **36**:1–61.
3. Deconick A, Koren B. *Euler and Navier–Stokes Solver Using Multi-Dimensional Upwind Schemes and Multigrid Acceleration*, Notes on Numerical Fluid Mechanics, vol. 57. Vieweg, 1997.
4. Hughes TJR, Tezduyar TE. Finite element methods for first-order hyperbolic systems with particular emphasis on the compressible Euler equations. *Computer Methods in Applied Mechanics and Engineering* 1984; **45**: 217–284.
5. Pironneau O. *Finite Element Methods for Fluids*. Wiley: New York, 1989.
6. Lohner R. *Applied CFD Techniques*. Wiley: New York, 2001.
7. Johnson FT, Tinco EN, Yu NJ. Thirty years of development and application of CFD at Boeing commercial airplanes. *AIAA Paper 2003-3439*, Seattle.
8. Hafez MM, Whitlow W, Osher S. Improved finite difference schemes for transonic potential calculations. *AIAA Journal* 1987; **25**(11):1456–1462.
9. Hafez MM, Guo WH. Simulation of steady compressible flows based on Cauchy/Riemann equations and Crocco's relation, Part I: inviscid flows. *International Journal for Numerical Methods in Fluids* 1998; **27**: 127–138.
10. Hafez MM, Guo WH. Simulation of steady compressible flows based on Cauchy/Riemann equations and Crocco's relation, Part II: Viscous flows. *International Journal for Numerical Methods in Fluids* 1999; **31**: 325–343.
11. Tang C, Hafez MM. Numerical simulation of steady compressible flows using a zonal formulation. Part I: inviscid flows. *Computers and Fluids* 2001; **30**.
12. Tang C, Hafez MM. Numerical simulation of steady compressible flows using a zonal formulation. Part II: Viscous flows. *Computers and Fluids* 2001; **30**.
13. Johnson FT, Bussoletti JE, Woo AC, Young DP. A transonic rectangular grid embedded panel method. *Advances in Computational Transonics*. Pineridge Press: Swansea, 1985.
14. Gordnier RE, Rubin SG. Transonic flow solutions using a composite velocity procedure for potential, Euler and RNS equations. *Computers and Fluids* 1989; **17**:85–98.
15. Hafez MM, Lovell D. Transonic small disturbance calculations including entropy corrections. *Numerical and Physical Aspects of Aero Flows Conference*. Springer: Berlin, 1981.
16. Hafez MM, Lovell D. Entropy and vorticity corrections for transonic flows. *International Journal for Numerical Methods in Fluids* 1988; **8**:31–53.
17. Roe P, Rad M. A form of the Euler equation conserving potential flow. *AIAA Paper 99-3280*.
18. Carter J. Viscous-inviscid interaction analysis of transonic turbulent separated flows. *AIAA Paper 81-1241*.
19. Wigton L, Holt M. Viscous-inviscid interaction computations in transonic flow. *AIAA Paper 81-1003*.
20. Cebeci T, Chen L, Chang K. An interactive scheme for three-dimensional transonic flows. *Numerical and Physical Aspects of Aerodynamical Flows III* 1985; 412–431.
21. Veldman A, Lindhout J, Boer E, Somers M. Vistrafs: a simulation method for strongly interacting viscous transonic flow. *Numerical and Physical Aspects of Aerodynamical Flows IV*, 1990; 37–51.
22. Williams B, Smith P. Coupling procedures for viscous-inviscid interaction for attached and separated flows on swept and tapered wings. *Numerical and Physical Aspects of Aerodynamical Flows IV*, 1990; 53–70.

23. Bieterman MR, Bussoletti JE, Hilmers CL, Huffman WP, Johnson FT, Melvin RG, Young DP. Boundary layer coupling in a general configuration full potential code. *2nd European CFD Conference*, Stuttgart, Germany, September 1994.
24. Flores J, Holst T, Kaynak U, Gunky K, Thomas S. Transonic Navier–Stokes wing solution using a zonal approach: Part I. Solution methodology and code validation. *Technical Report*, *NASA TM-88248*, 1986.
25. Flores J, Chaderjian N. Zonal Navier–Stokes methodology for flow simulations about complete aircraft. *Journal of Aircraft* 1990; **27**(7):583–590.
26. Sankar LN, Bharadvaj BK, Tsung F. Three dimensional Navier–Stokes/full potential coupled analysis for viscous transonic flow. *AIAA Journal* 1993; **31**(10):1857–1862.
27. Paraschivoiu M, Cai X, Sarkis M, Young DP, Keyes D. Multi-domain multi-model formulation for compressible flows: conservative interface coupling and parallel implicit solvers for 3D unstructured meshes. *AIAA Paper 99-0784*.
28. Quarteroni A, Valli A. *Domain Decomposition Methods for Partial Differential Equations*. Oxford Science Publications: Oxford, 1999.
29. Hafez MM, Wahba EM. Inviscid flows over a cylinder. *Computer Methods in Applied Mechanics and Engineering* 2004; **193**:1981–1995.
30. Cambier L. Computation of viscous transonic flows using an unsteady type method and a zonal grid refinement technique. In *Numerical Simulation of Compressible Navier–Stokes Flows: GAMM Workshop*, Bristeau MO, Glowinski R, Periaux J, Viviand H (eds). Vieweg, 1987; 105–122.
31. Kinney D, Hafez MM. Finite element simulation of compressible viscous flows over lifting airfoils. *AIAA paper 92-0669*, 1992.
32. Schroder W, Hanel D. An unfactored implicit scheme with multigrid acceleration for the solution of the Navier–Stokes Equations. *Computers and Fluids* 1987; **15**:313–336.
33. Hafez MM, Lovell D. Numerical solution of transonic stream function equation. *AIAA Journal* 1983; **21**: 327–335.
34. Sherif A, Hafez MM. Computation of three dimensional transonic flows using two stream functions. *International Journal for Numerical Methods in Fluids* 1988; **8**:17–29.

